ANNALS of Clinical and Translational Neurology
Open Access
ANA American Neurological Association since 1875

RESEARCH ARTICLE

Brain diabetic neurodegeneration segregates with low intrinsic aerobic capacity

Joungil Choi[1,2], Krish Chandrasekaran[1,2], Tyler G. Demarest[3], Tibor Kristian[2,3], Su Xu[4], Kadambari Vijaykumar[1,2], Kevin Geoffrey Dsouza[1,2], Nathan R. Qi[5], Paul J. Yarowsky[6], Rao Gallipoli[4], Lauren G. Koch[7], Gary M. Fiskum[3], Steven L. Britton[7] & James W. Russell[1,2]

[1]Department of Neurology, University of Maryland, Baltimore, Maryland 21201
[2]Veterans Affairs Medical Center, Baltimore, Maryland 21201
[3]Department of Anesthesiology, University of Maryland, Baltimore, Maryland 21201
[4]Department of Radiology, University of Maryland, Baltimore, Maryland, 21201
[5]Department of Internal Medicine, University of Michigan, Ann Arbor, Michigan 48109
[6]Department of Pharmacology, University of Maryland, Baltimore, Maryland 21201
[7]Department of Anesthesiology, University of Michigan, Ann Arbor, Michigan 48109

Correspondence
Joungil Choi, Department of Neurology, University of Maryland, School of Medicine, 655W. Baltimore Street, Bressler BLD 12-044, Baltimore, MD 21201. Tel: 410-706-5531; Fax: 410-706-0186; E-mail: jochoi@som.umaryland.edu

Funding Information
This work was supported in part by the Office of Research Development (Biomedical and Laboratory Research Service and Rehabilitation Research and Development, 101RX001030), Department of Veterans Affairs, NIH RR024888, the Juvenile Diabetes Research Foundation (JDRF), American Diabetes Association (ADA) (JWR), VA Baltimore Research and Education Foundation (JC), Veterans Administration Research and Development REAP award (JWR, JC), VA Biomedical Research Service Grant BX000917 (TK), National Institutes of Health grant 1S10RR19935 (RG, SX), and the Mid-Atlantic Nutrition Obesity Research Center, grant P30 DK072488 from the National Institute of Diabetes and Digestive and Kidney Diseases, National Institutes of Health. The LCR-HCR rat model system was funded by the National Center for Research Resources grant R24 RR017718 and is currently supported by the Office of Research Infrastructure Programs/OD grant ROD012098A (to L.G.K. and S.L.B.) from the National Institutes of Health. S.L.B. was also supported by National Institutes of Health grant RO1 DK077200. This work utilized 1) the Animal Phenotyping Core supported by Michigan Nutrition Obesity Research Center (DK 089503) and Michigan Diabetes Research and Training Center (NIH5P60

Abstract

Objectives: Diabetes leads to cognitive impairment and is associated with age-related neurodegenerative diseases including Alzheimer's disease (AD). Thus, understanding diabetes-induced alterations in brain function is important for developing early interventions for neurodegeneration. Low-capacity runner (LCR) rats are obese and manifest metabolic risk factors resembling human "impaired glucose tolerance" or metabolic syndrome. We examined hippocampal function in aged LCR rats compared to their high-capacity runner (HCR) rat counterparts. **Methods**: Hippocampal function was examined using proton magnetic resonance spectroscopy and imaging, unbiased stereology analysis, and a Y maze. Changes in the mitochondrial respiratory chain function and levels of hyperphosphorylated tau and mitochondrial transcriptional regulators were examined. **Results**: The levels of glutamate, *myo*-inositol, taurine, and choline-containing compounds were significantly increased in the aged LCR rats. We observed a significant loss of hippocampal neurons and impaired cognitive function in aged LCR rats. Respiratory chain function and activity were significantly decreased in the aged LCR rats. Hyperphosphorylated tau was accumulated within mitochondria and peroxisome proliferator-activated receptor-gamma coactivator 1α, the NAD^+-dependent protein deacetylase sirtuin 1, and mitochondrial transcription factor A were downregulated in the aged LCR rat hippocampus. **Interpretation**: These data provide evidence of a neurodegenerative process in the hippocampus of aged LCR rats, consistent with those seen in aged-related dementing illnesses such as AD in humans. The metabolic and mitochondrial abnormalities observed in LCR rat hippocampus are similar to well-described mechanisms that lead to diabetic neuropathy and may provide an important link between cognitive and metabolic dysfunction.

DK20572) and 2) the Chemistry Laboratory of the Michigan Diabetes Research and Training Center (NIH5P60 DK20572).

Received: 2 December 2013; Revised: 16 June 2014; Accepted: 20 June 2014

***Annals of Clinical and Translational Neurology* 2014; 1(8): 589–604**

doi: 10.1002/acn3.86

Introduction

Obesity and type II diabetes are among the fastest growing epidemics in modern times.[1] Convincing clinical, epidemiological, and genetic studies have provided substantial evidence supporting a link between type 2 diabetes and neurodegenerative diseases such as Alzheimer's disease (AD).[2–4] It is also suggested that AD may represent a consequence of a distinct form of brain-specific insulin resistance and impaired glucose regulation. In the Rotterdam study of 6370 elderly subjects, 126 developed dementia of which 89 specifically had AD.[5] Type 2-diabetes (T2DM) doubled the risk of a patient having dementia and patients on insulin had four times the risk.[5] Even in patients who do not have AD or diabetes, the presence of a mild increase in the high average glucose (6.4 mmol/L as compared with 5.5 mmol/L) over a moderate period of time significantly increases the risk of dementia.[6] This increased risk of dementia is of considerable impact on societies already facing epidemic levels of diabetes and impaired glucose tolerance.

Dysfunctional aerobic energy metabolism has been implicated in diabetes and age-related neurodegenerative disease. To study the contribution of aerobic exercise capacity to the etiology of complex disease states such as AD, we have developed animal models generated by artificial selection for low and high aerobic exercise capacity.[7] In these animal models, 11 generations of selection resulted in a 347% difference in running capacity between LCR and HCR rats.[7] LCR rats have impaired metabolic function, including obesity, insulin resistance, and dyslipidemia.[8] In LCR rats, there is a significantly low metabolic flexibility.[9] In contrast, HCR rats are lean and have a nonpathologic metabolic profile.

Neuronal loss, cognitive decline, hypometabolism, mitochondrial abnormality, and accumulation of hyperphosphorylated (p-Tau) have been reported in AD brain.[10,11] Microtubule-associated protein tau is critical for normal neuronal activity in the brain. Tau is abnormally hyperphosphorylated (p-Tau) in the brains of AD and experimental diabetes, which is associated with degeneration of neurons and cognitive impairment.[12–14] Mitochondrial abnormalities are found in diabetes and neurodegenerative diseases including AD.[11,15,16] Previous studies have showed a reduction in glucose metabolism and a deficiency in respiratory chain complexes including complex III in diabetes and AD patients.[10,17–19] PGC-1α, SIRT1, and TFAM are recognized to have a primary role in mitochondrial biogenesis and oxidative phosphorylation. Reduced PGC-1α expression is shown to be linked to insulin resistance, type 2 diabetes, and neurodegenerative disease.[20–23] PGC-1α overexpression protects neurons against oxidative stress by inducing antioxidant enzymes.[24] A recent study demonstrates that a novel brain PGC-1α isoform (35 kDa) localizes to hippocampal mitochondria and is associated with PTEN-induced putative kinase 1 (PINK1) and voltage-dependent anion channel, suggesting a possible new regulatory role for mitochondrial function in brain.[25] TFAM is the main determinant of the quantity of mitochondrial DNA.[26] In the TFAM knockout mice, there is a severe reduction in mitochondrial DNA, disruption of the electron transport chain, and increased mitochondrial oxidative stress.[27] Recent publications demonstrate that elevated SIRT1 levels have implications for the treatment of type II diabetes, and prevention of neurodegenerative diseases.[28–30] The putative benefits of exercise for maximizing cognitive function and supporting brain health have great potential for combating AD.[31] We conclude that aerobic exercise may reduce AD symptoms and appears effective in decreasing caregiver distress.[32]

To study the contribution of intrinsic aerobic exercise capacity upon aging to hippocampal integrity, we measured hippocampal volume, neuronal number, metabolic profile, mitochondrial function, and neurobehavioral studies. Here, we demonstrate that metabolic impairments resulting from genetic factors (selection on low intrinsic aerobic capacity) upon aging lead to hippocampal neurodegeneration, similar to AD. Furthermore, this study suggests mitochondrial dysfunction as a potential mechanism for hippocampal neuronal loss in LCR rats.

Materials and Methods

Animals

All animal procedures were approved by the Institutional Animal Care and Use committee at the University of Maryland School of Medicine, the VA Maryland Health Care System, and the University of Michigan and were in accordance with the NIH Guide for the Care and Use of Laboratory Animals. LCR and HCR rats were derived from genetically heterogeneous N:NIH stock rats by artificial selection for low and high treadmill running capacity as described previously.[7] Rats were phenotyped for intrinsic (i.e., inborn) running capacity at 11 weeks of age using an incremental treadmill running test. The single best daily run of three trials for each rat was considered the trial most closely associated with the heritable component of endurance running capacity and used to calculate aerobic exercise capacity in the form of work performed (joules). Rats were housed under approved conditions with a 12-h light/dark cycle with free access to food and water. Animals were provided with standard chow diets and water ad libitum. Aged male LCR and HCR rats (~25 months old) were used for this study.

Metabolic measurements

Metabolic studies were conducted by the University of Maryland School of Medicine Mid-Atlantic Nutrition Obesity Research Core and University of Michigan Animal Phenotyping Core. Mice were euthanized and blood was collected. The blood was centrifuged and plasma collected. A 50-μL sample from each mouse was collected for glucose, insulin, cholesterol, and triglyceride measurements using a colorimetric kit (Diagnostic Chemicals Ltd.,Waltham, MA U.S.A.). Oxygen consumption (VO_2), carbon dioxide production (VCO_2), and spontaneous motor activity were measured using the Comprehensive Laboratory Monitoring System (CLAMS; Columbus Instruments, Columbus, OH, U.S.A), an integrated open-circuit calorimeter equipped with an optical beam activity monitoring device. The CLAMS measurements were carried out continuously for 48–72 hours. Respiratory quotient (RQ) was calculated as ratio of VCO_2/VO_2. Body composition was measured using an NMR analyzer (Minispec LF90II; Bruker Optics, Watertown, MA, U.S.A.).

In vivo MRS/MRI experiments

In vivo MRS experiments were performed on a Bruker BioSpec 70/30USR Avance III 7T horizontal bore MR scanner (Bruker Biospin, MRI GmbH, Rheinstetten, Germany) equipped with a BGA12S gradient system and interfaced to a Bruker Paravision 5.0 console. A Bruker four-element ^{1}H surface coil array was used as the receiver and a Bruker 72-mm linear-volume coil as the transmitter. The rat was anesthetized in an animal chamber using a gas mixture of O_2 (1 L/min) and isoflurane (2.5%). The animal was then placed prone in an animal holder and the RF (radio frequency) coil was positioned and fixed over the brain of the animal. The animal holder was moved to the center of the magnet and the isoflurane level was changed to 2%. The level of isoflurane was further adjusted based on the respiration rate changes of the animal for the remainder of the experiment. A MR compatible small-animal monitoring and gating system (SA Instruments, Inc, Stony Brook, NY, U.S.A.) was used to monitor the animal respiration rate and body temperature. The animal body temperature was maintained at 36–37°C using warm water circulation. A three-slice (axial, mid-sagittal, and coronal) scout using a fast low angle shot (FLASH) sequence[33,34] was obtained to localize the rat brain. A fast shimming procedure (FASTMAP) was used to improve the B_0 homogeneity in the region of interest.[35] Both proton density- and T_2-weighted images were obtained using a 2D rapid acquisition with relaxation enhancement (RARE) sequence[36] in the axial plane of the brain with $TR/TE_{eff1}/TE_{eff2}$ = 5500/9.56/47.82 msec, RARE factor = 4, field of view (FOV) = 30 × 25 mm^2, slice thickness = 1 mm, in-plane resolution = 117 × 117 μm^2, number of averages = 1 for anatomic references. For ^{1}H MRS, adjustments of all first- and second-order shims over the voxel of interest were accomplished with the FASTMAP procedure. A Bruker outer volume suppression combined with point-resolved spectroscopy (PRESS) sequence[37] was used for signal acquisition from left and right hippocampus, respectively, with the voxel size of 3 × 3 × 3 mm. The rest of the parameters were TR/TE = 2500/20 msec, spectral bandwidth = 4 kHz, number of data points = 2048, number of averages = 320.

We performed volumetric MRI studies to reveal differences in hippocampal volume between the LCR and HCR rats. High-resolution multislice two-dimensional (2-D) volumetric MRI was used to elucidate structural changes present in the hippocampus of LCR and HCR rats. We used coronal sections to manually outline regions of interest (ROIs), including the dorsal hippocampus and the lateral and basolateral amygdalae from the both hemispheres. ImageJ (wsr@nih.gov) was used as the software package for image processing. Anatomical information was obtained from the Paxinos and Watson rat brain atlas.[38] Using the atlas-based segmentation approach, we computed the volume of the hippocampus for each animal. The protocol for measuring the hippocampal volume

was performed as previously described.[39] Drawings were made using a twofold magnification to construct the ROI, and checked at original size to determine accuracy. ROIs were only constructed on slices in which the hippocampal structure was visually and reliably distinct. Thus, although part of CA3 and the subiculum was visible beyond the respective rostral and caudal boundaries, they were not included in the analyses for the purpose of reliability. The hippocampus was measured on five consecutive slices in all animals, over a distance of roughly −2.16 mm to −7.20 from Bregma. The slices were examined from rostral to caudal. The narrowing of the ventral hippocampal commissure, the rounding of the dorsal third ventricle, and the appearance of both CA3 and the dentate gyrus was taken to represent the rostral boundary of the hippocampus. Measurement of hippocampal volume started around −2.16 mm from the Bregma and ended around −7.20 mm from the Bregma. Volumes were measured in pixels.

Stereological cell counting

We used the unbiased stereological methods and a computer-assisted system (Stereo Investigator; MicroBrightfiled Bioscience, Williston, VT, U.S.A) coupled to an Olympus microscope to obtain estimates of the total number of neurons in five major subdivisions of the mouse hippocampus as described previously.[40] The system uses a three-dimensional probe for counting neuronal nuclei called the optical dissector and a systematic uniform sampling scheme called the fractionators. Hippocampal sections (40 μm) were placed sequentially in wells and stained with cresyl violet. The reference point for the start of the measurement grid (260 × 80 mm) was the neuron from the CA1 closest to the corpus callosum. Neurons were counted at 100× amplification.

Spontaneous spatial novelty preference test on the Y maze

The LCR and HCR rats had no previous experience of any maze testing. The spontaneous spatial novelty preference test was conducted using a Y maze. Rats were assigned two arms ("start arm" and "other arm"), to which they were exposed for 5 min during the first phase of the test (the exposure phase). During this exposure phase, the entrance to the third arm of the maze was blocked. The rat was removed from the maze and returned to its home cage for 2 min. The rat was then returned to the maze for the test phase (10 min), during which it now had ad libitum access to all three arms of the maze. Entry into an arm was defined when a rat placed all four paws into an arm. A rat was considered to have left arm if all four paws were placed outside that arm. The amount of time a rat spent in each of the arms of the maze and the number of entries into each arm was recorded during both the exposure and test phases. For the test phase, a discrimination ratio (novel arm/[novel arm + other arm]) was calculated for both arm entries and time spent in arms.

Isolation of brain mitochondria

Hippocampal mitochondria from rat brain were isolated using a Percoll (Amersham Biosciences, Piscataway, NJ) gradient centrifugation as described previously.[25] Briefly, hippocampal tissue of rat brain was homogenized in ice-cold mannitol–sucrose (MS) buffer (225 mmol/L mannitol, 75 mmol/L sucrose, 5 mmol/L HEPES, 1 mmol/L EGTA, 1 mg/mL fatty-acid-free bovine serum albumin [BSA], pH 7.4 at 4°C). The homogenate was centrifuged at 1300 *g* for 3 min, and the pellet was resuspended and centrifuged again at 1300 *g* for 3 min. The pooled supernatants was centrifuged at 22,200 *g* for 8 min, the crude mitochondrial pellet was resuspended in 15% Percoll, and layered on a pre-formed gradient of 40% and 24% Percoll. After centrifugation at 31,700 *g* for 8 min, the mitochondria were collected from the interface of the lower two layers, diluted with isolation medium, and centrifuged at 16,700 *g* for 10 min. The purity of Percoll-isolated mitochondria was further confirmed by transmission electron microscopy and western blot analysis with various subcellular protein markers. The Percoll-purified mitochondrial pellet was used for respiratory chain complex assay and western blot analysis. For measuring respiration, the crude mitochondrial pellet, containing primarily free (nonsynaptic) mitochondria plus synaptosomes, was then resuspended in 10 mL of MS buffer, using gentle trituration with a disposable Pasteur pipette. A 13.5 μL of 10% (wt/vol) digitonin (Calbiochem, Billerica Massachusetts U.S.A.) in dimethylsulfoxide (DMSO) was added and gently mixed on ice for 3 min. This suspension material was spun at 22,000 *g* for 8 min. The mitochondrial pellet was then resuspended to a final volume of 1.5 mL of MS buffer plus BSA and centrifuged at 22,000 *g* for 10 min at 4°C in a microfuge. The resulting mitochondrial pellet was resuspended in MS without EGTA. Protein concentrations were determined in triplicate by standard Bradford method employing a BSA standard curve.

Mitochondrial respiration

Isolated mitochondria were added at a final concentration of 0.5 mg protein/mL to a thermostatically controlled O_2 electrode chamber (Hansatech Instruments, Norfolk,

England) equipped with magnetic stirring and containing 0.5 mL of respiration buffer (125 mmol/L KCl, 20 mmol/L Hepes and 2 mmol/L K_2HPO_4 at pH 7.4, 37°C). Malate and Glutamate were used as substrates to assess Complex I-mediated respiration. State 3 respiration was initiated by the addition of 1.0 mmol/L ADP. Approximately 2 min later, state 3 respiration was terminated and state 4_o respiration (resting) was initiated with addition of 1.25 μg/mL oligomycin, an inhibitor of the mitochondrial ATP synthase. The maximal rate of uncoupled respiration was subsequently measured by the addition of 65 nmol/L carbonyl cyanide p-(trifluoromethoxy)phenylhydrazone (FCCP), which is a protonophore uncoupling molecule. Rates are an average of 4–6 independent experiments for complex I respiration. One of seven experiments was excluded from analysis because respiratory rates were >2.7 and 16.7 standard deviations from the mean for HCR and LCR state 3 respiration, respectively. Rates between HCR and LCR hippocampi were statistically compared using a two-way unpaired Student's *t*-test. $P < 0.05$ was considered significant.

Carbonate extraction assay

The mitoplast was prepared followed by a carbonate extraction assay as described previously.[25] Mitochondria were resuspended in buffer A 10 mmol/L phosphate buffer, pH 7.4, 1 mmol/L ethylene glycol-bis (β-aminoethyl ether)*N*,*N*,*N*,*N*-tetraacetic acid (EGTA), 1 mmol/L PMSF, using a Dounce homogenizer, further diluted to a protein concentration of ~0.1 mg/mL, and kept on ice for 20 min. Mitoplasts were resuspended in buffer A containing 8.6% (w/v) sucrose and recovered from the 33%/47% interphase, washed and resuspended in buffer B (20 mmol/L 3-(*N*-morpholino) propanesulfonic acid, pH 7.2, 1 mmol/L EGTA, 1 mmol/L PMSF), and broken by freeze/thaw cycles followed by sonication. The inner membrane and matrix fractions of the mitoplasts were separated by centrifugation at 100,000 *g* for 30 min. The inner membrane fraction was further subjected to alkaline treatment (0.1 mol/L Na_2CO_3, pH 11.5 for 30 min) and then centrifuged at 144,000 *g* at 4°C to obtain integral inner membrane proteins.

Respiratory chain complex assay

Respiratory chain complex activity was measured on native protein complexes from purified rat hippocampal mitochondria using 3–12% native-PAGE as described previously.[41] Briefly, purified mitochondrial proteins (100 μg) were solubilized with 150 μL of buffer (50 mmol/L NaCl, 50 mmol/L imidazole/HCl, 2 mmol/L 6-aminohexanoic acid, 1 mmol/L EDTA, pH 7.0) containing a dodecyl-β-D-maltoside (Sigma, St. Louis, MO U.S.A) to a final concentration of 2.5 g per g protein. After incubation for 30 min on ice, samples were centrifuged at 20,000 *g* for 20 min and were supplemented with 20 μL of 50% (w/v) glycerol, 0.1% Ponceau S. Equal sample amount (20 μg) was applied to native gel (Invitrogen, Grand Island, NY, U.S.A.). The anode buffer (25 mmol/L imidazole/HCl, pH 7.0) and cathode buffer (50 mmol/L tricine, 7.5 mmol/L imidazole, 0.05% sodium deoxycholate, pH 7.0) were used for native electrophoresis. The native gel was used for in-gel catalytic activity assay. The gel was assayed for complex I activity in assay buffer (25 mg of nitrotetrazolium blue [NTB] and 100 μL of NADH [10 mg/mL] added to 10 mL of 5 mmol/L Tris/HCl, pH 7.4). After 3–10 min the reaction was stopped using the fixing solution (50% methanol, 10% acetic acid) and scanned for densitometric quantitation. For complex II assay, the gel was incubated with assay buffer containing 200-μL sodium succinate (1 mol/L), 8 μL of phenazine methosulfate (250 mmol/L dissolved in DMSO), and 25 mg of NTB in 10 mL of 5 mmol/L Tris/HCl, pH 7.4. After 30 min of incubation the reaction was stopped in fixing solution and scanned for densitometric quantitation. Complex III activity was analyzed by incubating the gel in complex III assay buffer (5 mg of diaminobenzidine dissolved in 10 mL of 50 mmol/L sodium phosphate, pH 7.2). After 60 min of staining, the gel was scanned for densitometric quantitation. For complex IV assay, the gel was incubated with the complex III assay buffer supplemented with 100 μL of horse heart cytochrome *c* (5 mmol/L) for 30 min followed by densitometric quantitation.

Mitochondrial DNA copy number and mitochondrial DNA damage

Genomic DNA was isolated from the hippocampus of LCR and HCR rat brains. Mitochondrial DNA copy number was determined by PCR of two mtDNA targets: a 197-bp ND1 gene and a 199-bp CytB gene and the Ct values were compared with a standard plasmid carrying ND1 and CytB mtDNA fragments. Nuclear DNA copy number was determined by PCR for a nuclear DNA 175-bp B2M gene target and the Ct values were compared with a plasmid carrying a B2M nuclear gene fragment. The ratio of mtDNA/nDNA was calculated by 2 × (ND1 Copies/20 ng DNA)/(B2M Copies/20 ng DNA); and by 2 × (CytB Copies/20 ng DNA)/(B2M Copies/20 ng DNA). Damage to mtDNA was measured by long-range (LR) Q-PCR of an 8.9-kb mtDNA target. This was based upon the principle that DNA damage slows down or blocks the progression of DNA polymerase along a template. PCR product was generated at three different

DNA concentrations to ensure the amplification was in the exponential phase and the products were quantified by PicoGreen fluorometry. The amount of PCR product was quantified and the amount is inversely related to mtDNA damage.

Western blot analysis of mitochondria

Purified mitochondria were incubated with protease K (for 25 min at 0°C) to remove the cytosolic proteins loosely associated with the outer mitochondrial membrane. The purified mitochondrial pellet was lysed in a buffer containing 50 mmol/L HEPES, 100 mmol/L NaCl, 1% NP-40, and a mixture of protease inhibitors (Roche Molecular Biochemicals, Mannheim Germany) and phosphatase inhibitors (Sigma). After homogenizing with 20 strokes using a Dounce homogenizer (Bellco Glass, Vineland, NJ, U.S.A.), mitochondrial lysates were centrifuged at 20,000 *g*, and the supernatants were used for western blot analysis with anti-PGC-1α,[25] anti-SIRT1 (sc-15404; Santa Cruz Biotechnology, Dallas, Texas, U.S.A.), anti-TFAM (NBP1-71648; Novus Biologicals, Littleton, CO, U.S.A.), anti-pTau Ser404 (sc-12952; Santa Cruz Biotechnology), anti-pTau Ser396 (44752; Invitrogen), anti-pTau Ser262 (ab131354; AbCam, Cambridge, MA. U.S.A.), anti-pTau Thr 231 (AB 9668; Millipore, Billerica, MA, U.S.A.), anti-Histone H3 (ab1791; AbCam), anti-GAPDH (2118; Cell Signaling), or anti-HSP 60 (4870; Cell Signaling) antibodies. Horseradish peroxidase-conjugated secondary antibodies were purchased from Pierce Biotechnology, Rockford, IL, U.S.A. Antibody binding was detected by using the SuperSignal chemiluminescence kit (Pierce) and an Alpha, Innotech imaging system (Santa Clara, California, U.S.A).

Immunoelectron microscopy

LCR and HCR rats were perfused with saline followed by 4% paraformaldehyde in 0.1 mol/L of phosphate buffer. Rat hippocampus tissue was dissected under an operating microscope, mounted in the slot of a small screw, and snap frozen in liquid nitrogen. Ultrathin sections (70–100 nm) from rat hippocampus tissue were incubated concurrently with primary antibodies against p-Tau Ser404 (1:50) or Ser396 (1:50) for 1 h and followed by incubation with appropriate 10 nm immunogold-conjugated secondary antibodies (Jackson ImmunoResearch, Laboratory, West Grove, PA, U.S.A.) for 1 h. Sections were fixed with 2.5% glutaraldehyde, counterstained with 4% neutral uranyl acetate, embedded in 1.25% methyl cellulose, then observed using a JEOL JEM 1210 electron microscope (JEOL USA, Inc, Peabody, MA, U.S.A.) at 80 kV.

Statistics

The results are presented as mean ± SEM. A statistical analysis was performed based on two-tailed *t*-test with the significance level at $P \leq 0.05$ or $P \leq 0.001$.

Results

Whole-body metabolic parameters

When young, the LCR and HCR rats differ by 6-fold for intrinsic aerobic running capacity, aged LCR were significantly more obese than HCR, as indicated by higher body weight and percent body fat (Table 1, $P < 0.001$). The value of VO_2 over 24 h, corrected for lean body mass, an indicator of energy expenditure, was significantly lower in the LCR than the HCR rats (Table 1, $P < 0.001$) but there was no difference in the RQ between LCR and HCR rats. Both fasting and nonfasting glucose were significantly higher in the LCR than HCR rats (Table 1, $P < 0.001$).

^{1}H MRS

LCR and HCR rats were subjected to in vivo ^{1}H MRS of the dorsal hippocampus. ^{1}H MRS allows the noninvasive assessment of altered brain metabolic profile[42] and measurement of the biomechanical changes associated with central nervous system injury.[43] All data were analyzed using the LC-Model package[44] and the results are shown (Fig. 1). There was a significant difference in the hippocampal MRS metabolic profile between LCR and HCR rats. Creatine and phosphocreatine (Cr) were used as the internal standard for comparison because they remain relatively

Table 1. Metabolic values in HCR and LCR rats.

	HCR (N = 10)	LCR (N = 10)
Body weight (g)	407.69 ± 9.46	577.01 ± 25.67*
Percent body fat	12.06 ± 0.71	23.40 ± 1.21*
VO_2 over 24 h corrected for lean body mass (mL/kg)	1674.40 ± 33.50	1447.0 ± 39.70*
Respiratory quotient (VCO_2/VO_2) over 24 h	0.90 ± 0.01	0.90 ± 0.02
Fasting glucose (mg/dL)	67.27 ± 1.94	82.72 ± 2.27*
Nonfasting glucose (mg/dL)	97.1 ± 2.65	115.6 ± 4.27*
Insulin (ng/mL)	0.62 ± 0.19	0.93 ± 0.36
Triglyceride (mg/dL)	87.64 ± 12.59	98.23 ± 58.41
Cholesterol (ng/mL)	1.36 ± 0.18	1.54 ± 0.18
HDL cholesterol (μg/mL)	0.88 ± 0.15	0.74 ± 0.08

The rest of the comparisons are not statistically different. VO_2, oxygen consumption; VCO_2, CO_2 production; HDL, high-density lipoprotein.
*$P < 0.001$ as compared to HCR.

A

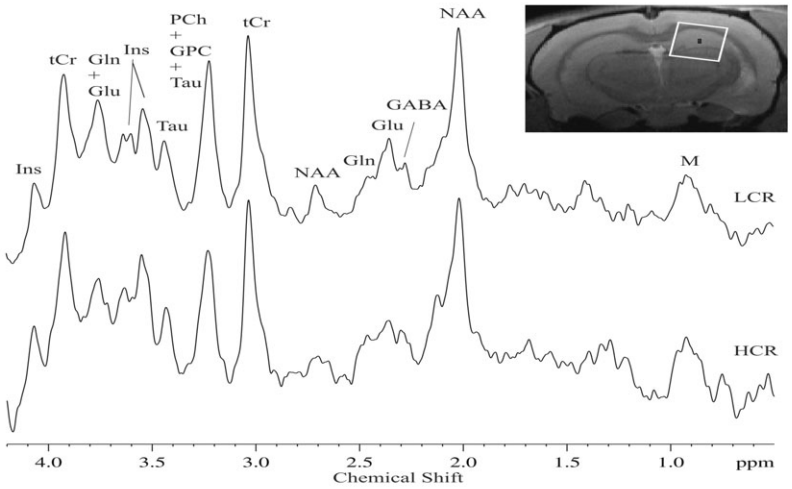

B

Neurochemical profile in the hippocampus of LCR and HCR rats

METICr + Pcr	LCR	HCR	P
Glucose	0.66	0.78	0.13
Glutamine	0.81	0.93	0.08
Glutamate	1.01	0.87	0.0057
Myoinositol	1.17	1.02	0.0012
NAA	0.747	0.76	0.302
Taurine	0.7	0.52	<0.0001
Glycerophosphorylcholine & phosphorylcholine	0.242	0.22	0.0074

NAA: N-acetylaspartate

Figure 1. Concentrations of metabolites in the dorsal hippocampus are altered in LCR rats compared to HCR rats. (A) Example of spectrum from the dorsal hippocampus of a LCR rat (top) and an HCR rat (bottom). (B) Neurochemical profile of LCR and HCR rats (N = 9/group). The ratios of in vivo mean metabolite concentrations of glucose, glutamine (Gln), glutamate (Glu), *myo*-inositol (Ins), glycerophosphorylcholine (GPC) and phosphorylcholine (PCh), *N*-acetylaspartate (NAA), and Taurine (Tau) relative to total creatine (tCr) were computed for each voxel and a paired one-tail Student's *t*-test was performed to compare the difference between the neurochemical profiles of the LCR and the HCR rats. Data represent the mean ± SEM for spectra from the left and right hippocampus. LCR, low-capacity runner; HCR, high-capacity runner.

constant. The top panel of Figure 1 shows a representative ^{1}H MRS spectrum of LCR and HCR hippocampus. The glutamate/tCr ($P < 0.01$), *myo*-inositol/tCr ($P < 0.01$), taurine/tCr ($P < 0.0001$), and glycerophosphocholine and phosphocholine/tCr ($P < 0.01$) ratios were significantly higher in LCR than HCR rats (Fig. 1). A decreasing trend was observed in glutamine/tCr ($P < 0.08$) for the LCR rats compared to the HCR rats (Fig. 1). There was no difference in the glucose/tCr and *N*-acetylaspartate (NAA)/tCr ratios between LCR than HCR rats (Fig. 1).

Morphological MRI and histology of the hippocampus

Volumetric analysis showed a significant change in the relative sizes for ROIs analyzed in LCR rats versus HCR

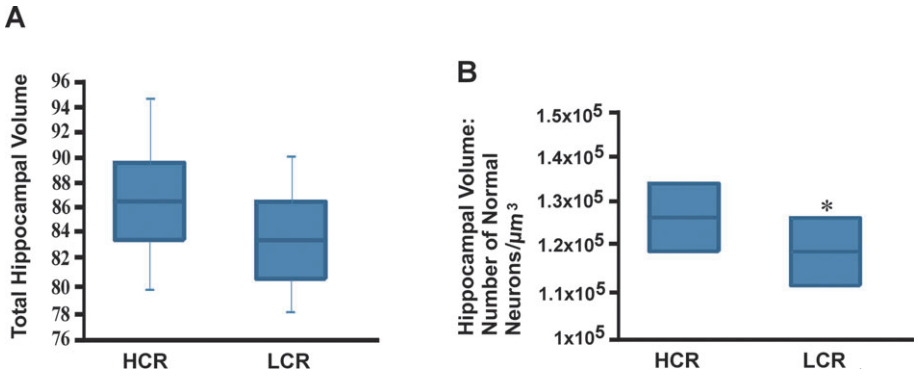

Figure 2. Hippocampal volume and neuronal number are reduced in LCR rats compared with HCR rats. (A) The total hippocampal volume on MRI (total volume for left and right hippocampus) was measured in LCR (N = 13) and HCR rats (N = 14). (B) Unbiased stereology measurement of the total volume of normal neurons in the CA1 region of the hippocampus shows that the neuron count is significantly reduced in LCR compared to HCR rats (N = 5). *P < 0.05. LCR, low-capacity runner; HCR, high-capacity runner.

rats. The mean total hippocampal volume of the LCR rats was markedly decreased compared to the HCR rats (Fig. 2A). Unbiased stereological cell counting confirmed significant cell loss in the CA1 region of LCR rats compared with HCR rats (Fig. 2B).

Spontaneous spatial novelty preference test on the Y maze

Using a Y maze, we determined differences in cognitive abilities dependent on hippocampal function between LCR and HCR rats. The Y maze assesses rapidly acquired, short-term spatial memory and relies on the fact that normal rats prefer novel over familial spatial environments. In this task, animals explored two arms and then were returned to the home cage. During the exposure phase, LCR and HCR rats made a similar number of total arm entries. The number of arm entries and the amount of time spent exploring the two arms (the start and other arms) did not differ. During the test phase, HCR rats, compared with LCR rats, showed a strong preference for the novel arm (previously unvisited arm). Discrimination ratio analysis showed that the LCR rats had less preference for the novel arm ($P < 0.05$) than the HCR rats (Fig. 3).

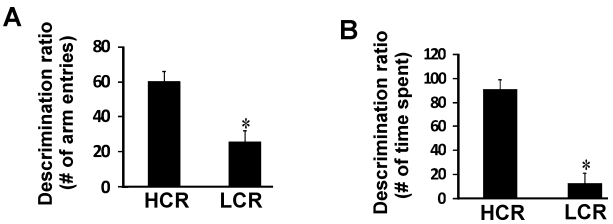

Figure 3. LCR rats display a reduced spatial novelty preference compared to HCR rats. A discrimination ratio (100 × novel/[novel + other]) was calculated for both the number of arm entries (A) and the time spent in the arm (B) for both LCR and HCR rats (N = 9). *P < 0.05. LCR, low-capacity runner; HCR, high-capacity runner.

Mitochondrial electron transport chain activity, function, mitochondrial DNA copy number, and mitochondrial DNA damage

Impairment of mitochondrial respiratory chain complex activity has been well documented in diabetes and AD patients.[10,18,19] Therefore, we measured the changes in the respiratory chain complex activity and respiratory function in hippocampal mitochondria between LCR and HCR rats. Using the mild nonionic detergent dodecy-β-D-maltoside (DDM), four complexes (complex I–IV) of mitochondrial oxidative phosphorylation were solubilized as individual membrane protein complexes, namely, NADH:ubiquinone reductase (complex I, ~740 kDa), succinate:ubiquinone reductase (complex II, ~200 kDa), ubiquinol:cytochrome *c* reductase (complex III, ~300 and 600 kDa), and cytochrome *c* oxidase (complex IV, ~240 and 620 kDa) (Fig. 4A). In comparison with the HCR rats, LCR rats had significantly lower hippocampal complex III activity (with mean reduction of 30%) (Fig. 4B). In contrast, LCR rats had a nonsignificant trend for lower complex I, II, and IV activities (with mean reduction of less than 5%) compared with HCR rats (Fig. 4B). We then performed isolated hippocampal mitochondrial respirometry at physiological temperature (37°C) to assess possible mitochondrial functional differences between HCR and LCR rats. Hippocampal mitochondria from LCR rats respiring on complex I substrates malate and glutamate had a slight but significantly decreased state 3 respiration ($P < 0.05$, mean reduction of 11.8%). A similar but nonsignificant reduction of ~10% was observed

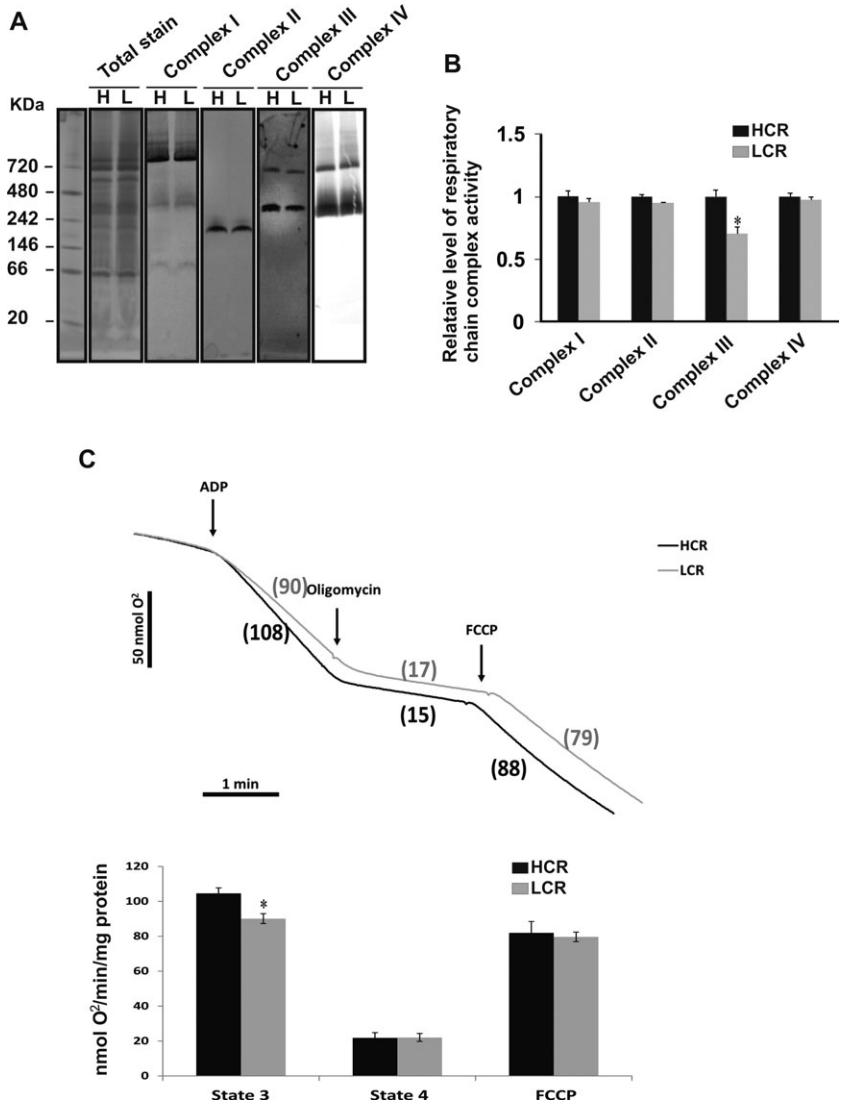

Figure 4. Reduced mitochondrial respiratory chain complex III activity and state 3 respiration in LCR rats compared with HCR rats. (A) Hippocampal mitochondria of LCR and HCR rats were solubilized with dodecyl-β-D-maltoside (DDM) and mitochondrial protein lysates (50 μg) were loaded onto the blue native gel wells. After electrophoresis, one gel was stained with Coomassie blue, the other gels were subjected to "In-gel activity analysis" to reveal the presence of complex I, II, III, or IV. H, HCR; L, LCR. (B) Densitometric quantification of each protein band ($N = 5$). *$P < 0.05$. (C) Oxygen consumption rates for hippocampal mitochondria isolated from LCR and HCR rats. Data are presented as the average OCR $\pm$ SE. *$P < 0.05$. LCR, low-capacity runner; HCR, high-capacity runner.

with complex II substrate succinate in the presence of complex I inhibitor rotenone. We also determined changes in mitochondrial DNA copy number and mitochondrial DNA damage (e.g., CytB gene) in the hippocampal mitochondria between LCR and HCR rats. Genomic DNA was isolated from hippocampus of LCR and HCR rat brains. Mitochondrial DNA copy number was determined by PCR of two mtDNA targets: a 197-bp ND1 gene and a 199-bp CytB gene. Mitochondrial DNA damage was measured by LR Q-PCR of an 8.9-kb mtDNA target. The results revealed that there is no significant difference in mitochondrial DNA copy number or mitochondrial DNA damage between LCR and HCR rats (Table 2).

Mitochondrial regulatory proteins and phospho-Tau

We determined whether the protein levels of PGC-1α, SIRT1, and TFAM, the major regulators of mitochondrial biogenesis and metabolism, are altered in LCR rats compared with HCR rats. Hippocampus tissues obtained from

Table 2. Mitochondrial DNA copy number and DNA damage in HCR and LCR rat.

Tissue	B2M copies/20 ng DNA	ND1 copies/20 ng DNA	Ratio (mtDNA/nDNA)
LCR	22,000 ± 2014	39,220,000 ± 120,000	1945 ± 224
HCR	21,500 ± 1960	38,750,000 ± 119,000	1897 ± 205
Tissue	B2M copies/20 ng DNA	CytB copies/20 ng DNA	Ratio (mtDNA/nDNA)
LCR	22,000 ± 2014	38,890,000 ± 121,000	2012 ± 205
HCR	21,500 ± 1960	37,967,000 ± 119,750	1978 ± 198
Tissue	LR DNA amplified	LR DNA amplified/10^6 ND1 copies	LR DNA amplified/10^6 CYTB copies
LCR	2088 ± 218	91 ± 10	88 ± 8
HCR	2175 ± 207	94 ± 12	91 + 9

LCR, low-capacity runner; HCR, high-capacity runner; LR, long range.

LCR and HCR rats were analyzed by western blotting using antibodies against PGC-1α, SIRT1, and TFAM (Fig. 5A). The results revealed that there is a significant decrease in PGC-1α (35 kDa), SIRT1, and TFAM protein levels in the hippocampus samples from LCR rats compared with HCR rats (Fig. 5B). Increased hyperphosphorylated tau (p-Tau) has been reported in diabetes.[14,45] Therefore, we determined whether p-Tau is increased in the hippocampus of LCR rats. Mitochondria were purified from the hippocampus of LCR and HCR rats. Purified mitochondria were treated with protease K to remove the cytosolic proteins that are loosely attached to the mitochondrial outer membrane and were subjected to western blot analysis with various anti-P-Tau (Ser404, Ser396, Ser262, and Thr231) antibodies. We verified the purity of the mitochondrial fraction using western blot analysis with anti-HSP60, Histon H3, and GAPDH antibodies (Fig. 5C), as well as transmission electron microscopy (Fig. 5E and F). Compared to the crude mitochondrial fraction that contains various subcellular organelles (Fig. 5E), we observed only mitochondria in the Percoll-purified mitochondrial fraction used for western blot analysis (Fig. 5F). Results showed that there is an accumulation of p-Tau (Ser404, Ser396, Ser262, and Thr231) in the hippocampal mitochondria of LCR but not HCR rats (Fig. 5C). We further investigated the submitochondrial localization of p-Tau by performing a carbonate extraction assay. The purified mitochondrial inner membrane and matrix fractions of the mitoplasts were subjected to western blot analysis with anti-p-Tau Ser404 antibody. Results showed a presence of p-Tau in the both soluble and pellet fractions (Fig. 5D). We verified the purity of the matrix fraction and the inner membrane fraction using western blot analysis with anti-Grp 75 (a mitochondrial matrix marker), anti-NDUFV2 (a mitochondrial inner membrane marker), anti-Histone H3, and anti-GAPDH antibodies.

Immunoelectron microscopy analysis of LCR and HCR hippocampal tissue with anti-p-Tau (Ser404 and Ser396) antibodies showed apparent localization of p-Tau protein in the mitochondria of LCR (Fig. 5G and H) but not HCR rats (Fig. 5I and J). To quantitatively estimate the immunogold labeling produced by the p-Tau Ser404 or Ser396 antibody, we counted the total number of immunogold particles observed within mitochondria (1173 or 1295 gold particles from 30 mitochondria of three pellets were counted total in the section labeled with p-Tau Ser404 or Ser396, respectively). Quantification data showed that 13 ± 3 or 14 ± 5 particles/mitochondria were observed in the section labeled with p-Tau Ser404 or Ser396, respectively. No gold particles were detected in the negative controls when the anti-p-Tau antibodies (Ser404 and Ser396) were omitted and secondary antibody included (data not shown). We also observed some p-Tau Ser404 and Ser396 immunoreactivities outside the mitochondria. We verified our immunoelectron microscopy analysis of LCR rat hippocampal tissue with anti-voltage-dependent anion channel (VDAC) antibody as a positive control (Fig. S1). Double labeling immunoelectron microscopy analysis with antibodies against p-Tau Ser396 or Ser404 and VDAC revealed that these two proteins colocalize in the hippocampal mitochondria of LCR rat brain (Fig. S1). We also verified the specificity of p-Tau Ser404 and Ser396 antibodies using western blot analysis (Fig. S2). Neither p-Tau Ser404 nor Ser396 immunoreactivity was detected in the controls, when the samples were pretreated with lambda protein phosphatase or antibodies were preincubated with phosphopeptide that was derived from human Tau around the phosphorylation site of serine 396 or 404 (Fig. S2).

Discussion

This study demonstrates that impaired cognitive function and neurodegeneration are observed in the hippocampus of aged LCR rats. In parallel to these abnormalities, there is an alteration in the hippocampal metabolic profile, a decrease in mitochondrial respiration, complex III activity, mitochondrial regulatory protein levels, and an accumulation of hyperphosphorylated Tau within mitochondria. Importantly, the aged LCR rats also exhibit many

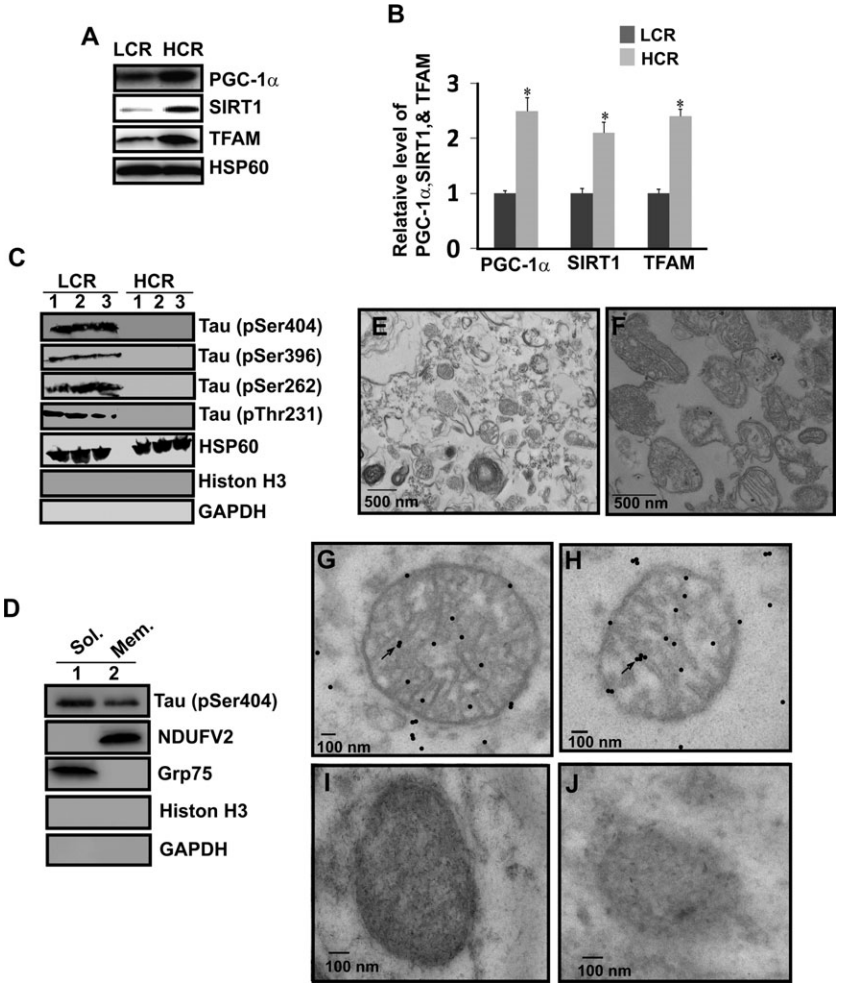

Figure 5. There is a significant decrease in the protein levels of PGC-1α, SIRT1, and TFAM in the hippocampus of LCR compared to HCR rats and an accumulation of hyperphosphorylated p-Tau in the hippocampal mitochondria of LCR but not HCR rats. (A) Total protein lysates (25 μg) from the hippocampus of LCR and HCR rats were subjected to SDS-PAGE gel followed by immunoblotting with anti-PGC-1α, SIRT1, TFAM, and HSP 60 antibodies. **(**B) Densitometric quantification and normalization to the HSP 60 level in the corresponding samples ($N = 5$). *$P < 0.05$. (C) Lysates (25 μg) from purified hippocampal mitochondria were subjected to SDS-PAGE gel followed by immunoblotting with various anti-phosphoTau (pSer404, pSer396, pSer262, and pThr231) antibodies. Lanes 1, 2, and 3 represent three different rats. (D) Western blot analysis of mitochondrial inner membrane (Mem.) and matrix (Sol.) probed with antibodies directed against pSer404, NDUFV2, Grp 75, Histone H3 (a nuclear marker), and GAPDH (a cytosolic marker). We verified the purity of the mitochondrial fraction using western blot analysis with anti-HSP60, Histone H3, and GAPDH antibodies (C and D), as well as transmission electron microscopy (E and F). Transmission electron microscopy of the crude mitochondrial pellet (E) and the Percoll-purified mitochondrial pellet (F) used for western blot analysis (C). (G, H, I, and J) Immunoelectron microscopy of mitochondrial hyperphosphorylated p-Tau Ser404 (G) and Ser396 (H) localization in the hippocampus of LCR rats. Black arrow indicates hyperphosphorylated p-Tau immunogold labeling. Neither hyperphosphorylated p-Tau Ser404 (I) nor Ser396 (J) immunoreactivity was detectable in the hippocampus of HCR rats. LCR, low-capacity runner; HCR, high-capacity runner.

characteristics common to humans with metabolic syndrome with mild type 2 diabetes mellitus. These include increased body weight and adiposity, increased fasting and nonfasting glucose, and decreased aerobic capacity (VO_2). Thus, this animal model presents a novel phenotype for cognitive decline and neurodegeneration that would model similar changes seen in human metabolic syndrome with mild type 2 diabetes mellitus.[4] Furthermore, the impaired mitochondrial function and reduced mitochondrial transcription factors would be consistent with a metabolic phenotype that results in impaired hippocampal neuronal function and degeneration. In addition to this possibility, previous studies indicated that mitochondrial function is impaired in skeletal muscle and liver in LCR rats[46,47] and presumably most if not all other locations. Therefore, it is axiomatic that the status of the hippocampus is an admixture of local and remote influences.

We observed a significant increase in glutamate/tCr in the hippocampus of live LCR rats compared with HCR rats. An increased extracellular glutamate concentration at the synapse level has been implicated in hippocampal cell death.[48,49] Accordingly, our unbiased stereological analysis and behavioral measurement showed a significant cell loss in the CA1 region and cognitive impairment in LCR rats compared with HCR rats. There were also increases in the *myo*-inositol/tCr and taurine/tCr ratios in the hippocampus of LCR rats compared with HCR rats. Previously, increased *myo*-inositol has been shown to be related to the activation of microglia in an animal model of AD.[50] Moreover, taurine has been shown to protect neurons against both Aβ- and glutamate receptor agonist-induced toxicity.[51,52] Interestingly, taurine is significantly increased in LCR rats. Taurine is an abundant amino acid present in brain, has antioxidant properties, and is known to act as an osmoregulator and regulator of mitochondrial function. Although taurine is decreased in AD brain, its chemical structure is similar to 3-amino-1-propanesulfonic acid, a compound which interferes with beta-amyloid peptide aggregation. Furthermore, taurine slightly decreases beta-amyloid peptide aggregation[53] and the high levels observed in LCR hippocampus would be consistent with a feedback response to ongoing neurodegeneration. Both *myo*-inositol and taurine are major osmolytes in the brain,[54,55] and thus an alteration in the levels of these metabolites could well indicate changes in cell volume regulation. Consistent with this concept, it has been reported that hippocampal volume in humans with AD is smaller than in controls and the degree of volume decrease is associated with greater severity of dementia.[56] Thus, the high levels of taurine and/or *myo*-inositol observed in LCR hippocampus may contribute to hippocampal volume loss in these animals. In accord with this possibility, we observed a significant decrease in hippocampal volume in LCR rats compared with HCR rats.

Alterations in membrane synthesis and degradation can produce changes in the glycerophosphocholine and phosphocholine/tCr peak, as these are breakdown products, and the latter is a precursor for phosphatidylcholine, a major component of cell membranes. Increased levels of glycerophosphocholine and phosphocholine have been previously reported in AD brain.[57] Similarly, we observed a significant increase in the glycerophosphocholine and phosphocholine/tCr peak in the hippocampus of LCR rats compared with HCR rats. Previously, inhibition of mitochondrial bioenergetics in neuronal cells has been shown to accelerate phosphatidylcholine synthesis and breakdown.[58] This suggests the presence of alterations in cell membrane regulation in the LCR rats, which may be implicated with changes in mitochondrial function in these animals.

In AD and diabetes patients, a neuronal loss in the CA1 region of hippocampus and cognitive impairment has been documented in many studies.[59,60] The medial prefrontal cortex receives projections directly from the intermediate CA1 region of the hippocampus and this link may be critical for spatial navigation.[61] Accordingly, we observed neuronal loss in the CA1 region of the hippocampus and impairment of spatial memory in the LCR rats compared with HCR rats. Consistent with our results, a recent study reported that in comparison with HCR rats, LCR rats show impaired cognitive function, but no impairment of motor running.[62] Overall, the findings demonstrate that prominent metabolite alterations occur in the hippocampus of LCR rats, which is similar to AD brains and may contribute to the development of hippocampal neurodegeneration including neuronal loss, decreased hippocampal volume, and cognitive dysfunction.

Previous studies in skeletal muscle and heart have shown that the selection for low- and high-running capacity led to significant differences in mitochondrial function and content between LCR and HCR rats.[8,63] Accordingly, our study in brain demonstrates that protein levels of key mitochondrial regulators, PGC-1α, SIRT1, and TFAM, were significantly decreased in LCR rats compared with HCR rats. SIRT1 activity increases deacetylation, activates downstream PGC-1α,[64] and also interacts with TFAM in the mitochondrion.[65] Both SIRT1 and PGC-1α play an important role in mitochondrial regeneration, cellular metabolism, and longevity.[64] TFAM is essential for transcription, replication, and maintenance of mtDNA.[64] SIRT1 protects neurons against β-amyloid-induced toxicity.[66] In part, SIRT1 neuroprotection may be because of improved energy homeostasis.[67] Interestingly, a T-to-C exchange in exon 1 of SIRT1, corresponding to a leucine-to-proline mutation at residue 107 results in metabolic dysfunction in humans[68] indicating that failure of the SIRT1–PGC-1α axis and TFAM, as observed in LCR rat hippocampal mitochondria, would further impair metabolic and mitochondrial function in neurons and aggravate neurodegeneration.

Hippocampal mitochondrial respiration on complex I substrates was significantly decreased in LCR rats compared to HCR rats, whereas complex II respiration was not significantly different. Respiratory chain complex III activity was significantly decreased in LCR rats. In contrast, respiratory chain complex I, II, or IV remained unchanged in these animals. Unfortunately, we were unable to determine respiratory chain complex V activity; however, the fact that the FCCP-stimulated uncoupled mitochondrial respiration was not different between LCR and HCR suggests a possibility of dysfunction at the level of complex V. Expression of complex III protein component is putatively controlled by PGC-1α, thus

reduced PGC-1α or SIRT1 could contribute to the observed reduction in complex III activity in LCR rats. Inhibition of complex III has been shown to cause glutamate release from the nerve terminal.[69] Our MRS data exhibited a significant increase in glutamate levels in LCR rats compared with HCR rats. This result suggests a correlation between complex III deficiency and potential glutamate-mediated excitotoxicity in LCR rats. In addition, the reduction in complex III activity in LCR would likely lead to a greater exposure to mitochondria-derived reactive oxygen species production and propagation of mitochondrial dysfunction due to mitochondrial DNA mutations. In accordance with this possibility, we observed a significant reduction in state 3 respiration rate in the hippocampus of LCR compared to HCR rats. This raises the possibility of lower energy metabolism due to impaired complex III activity and could be associated with the divergence in hippocampal integrity observed in the aged LCR and HCR rats. In support of this possibility, human pathological tissue studies have demonstrated that reduction in the activity of respiratory chain complex III and altered glucose metabolism are found in AD.[10,70] Interestingly, we observed that there was no significant difference in mitochondrial DNA copy number and DNA damage between LCR and HCR rats. These results, however, do not rule out the possibility that specific mutations in the CYTB gene could contribute to mitochondrial impairment in LCR brains. Given the well-established metabolic disease susceptibility of LCR rats, our results suggest that a reduced complex III activity, coupled with a reduced expression of transcriptional regulators, may play an important role in susceptibility to neurodegeneration, providing further evidence of the importance of the mitochondrial energy metabolism in brain function.

Interestingly, this study demonstrated a previously unreported deposition of hyperphosphorylated Tau in the mitochondria of LCR rats, but not in HCR rats. Tau protein binds and stabilizes microtubules, and hyperphosphorylation diminishes the ability of tau to bind microtubules, resulting in microtubule destabilization. In addition, unbound hyperphosphorylated tau may be localized to an abnormal subcellular region such as mitochondria, which could contribute to impaired electron transport chain function and activity observed in LCR rats. Previously, Tau transgenic mice have been shown to exhibit deposition of hyperphosphorylated Tau, and develop progressive age-related neurofibrillary tangles, hippocampal neurodegeneration, and behavioral impairments.[70–72] Experimental diabetes has been shown to exacerbate Tau pathology in a transgenic mouse model of AD.[45] Furthermore, mitochondrial dysfunction and oxidative stress cause hyperphosphorylation of Tau, and antioxidants that target mitochondria significantly reduce phosphorylated Tau.[73] These results suggest that metabolic and specifically mitochondrial alterations found in LCR brain may cause the increased hyperphosphorylation of Tau, which would likely contribute to the hippocampal neurodegeneration. Further research is required to determine the precise role of hyperphosphorylated Tau deposition in the LCR mitochondria.

This study demonstrates that aged LCR rats exhibit many AD features, including altered metabolism, mitochondrial abnormalities, neuronal loss, decreased hippocampal volume, and impaired cognitive function. Further research is required to determine the precise interplay and temporal relationship between the metabolic and mitochondrial abnormalities in the LCR rat hippocampus and neuronal dysfunction. The aged LCR/HCR models used in the present investigation provide novel evidence that metabolic dysfunction is associated with hippocampal neurodegeneration. This is in agreement with previous studies suggesting that defects in glucose, lipid, and insulin metabolism affect cognitive function. Furthermore, these metabolic defects may represent an early stage in the progression of some neurodegenerative diseases in humans such as AD. Given the fact that AD is sporadic with unclear pathogenesis in the majority of affected people, the abnormalities described in the LCR rat brain may represent early targets for further understanding the pathophysiology and potential interventions in this debilitating disease.

Acknowledgments

We thank Dr. Daniel Kelly and Ms. Theresa Leone for providing the PGC-1α antibody. We also thank Drs. Ying Han and Gary F. Gerard (Transgenomics Inc., Five Science Park, New Haven, CT 06511) for helping us to study mutations in CytB (CPT code 81479) and MITO-DEL (CPT code 81405). This work was supported in part by the Office of Research Development (Biomemedical and Laboratory Research Service and Rehabilitation Research and Development, 101RX001030), Department of Veterans Affairs, NIH RR024888, the Juvenile Diabetes Research Foundation (JDRF), American Diabetes Association (ADA) (JWR), VA Baltimore Research and Education Foundation (JC), Veterans Administration Research and Development REAP award (JWR, JC), VA Biomedical Research Service Grant BX000917 (TK), National Institutes of Health grant 1S10RR19935 (RG, SX), and the Mid-Atlantic Nutrition Obesity Research Center, grant P30 DK072488 from the National Institute of Diabetes and Digestive and Kidney Diseases, National Institutes of Health. The LCR-HCR rat model system was funded by the National Center for Research Resources grant R24

RR017718 and is currently supported by the Office of Research Infrastructure Programs/OD grant ROD012098A (to L.G.K. and S.L.B.) from the National Institutes of Health. S.L.B. was also supported by National Institutes of Health grant RO1 DK077200. This work utilized 1) the Animal Phenotyping Core supported by Michigan Nutrition Obesity Research Center (DK 089503) and Michigan Diabetes Research and Training Center (NIH5P60 DK20572) and 2) the Chemistry Laboratory of the Michigan Diabetes Research and Training Center (NIH5P60 DK20572). We acknowledge the expert care of the rat colony provided by Ms. Molly Kalahar and Ms. Lori Heckenkamp and the staff of the University of Michigan Metabolomics Core for their technical assistance. Contact L.G.K. (lgkoch@med.umich.edu) or S.L.B. (brittons@umich.edu) for information on the LCR and HCR rats: these rat models are maintained as an international collaborative resource at the University of Michigan, Ann Arbor.

Conflict of Interest

None declared.

References

1. Caballero B. The global epidemic of obesity: an overview. Epidemiol Rev 2007;29:1–5.
2. Strachan MW, Price JF, Frier BM. Diabetes, cognitive impairment, and dementia. BMJ 2008;336:6.
3. Cole AR, Astell A, Green C, et al. Molecular connexions between dementia and diabetes. Neurosci Biobehav Rev 2007;31:1046–1063.
4. Grunblatt E, Bartl J, Riederer P. The link between iron, metabolic syndrome, and Alzheimer's disease. J Neural Transm 2011;118:371–379.
5. Ott A, Stolk RP, van Harskamp F, et al. Diabetes mellitus and the risk of dementia: The Rotterdam Study. Neurology 1999;53:1937–1942.
6. Crane PK, Walker R, Hubbard RA, et al. Glucose levels and risk of dementia. N Engl J Med 2013;369:540–548.
7. Koch LG, Britton SL. Artificial selection for intrinsic aerobic endurance running capacity in rats. Physiol Genomics 2001;5:45–52.
8. Wisloff U, Najjar SM, Ellingsen O, et al. Cardiovascular risk factors emerge after artificial selection for low aerobic capacity. Science 2005;307:418–420.
9. Koch LG, Britton SL, Wisloff U. A rat model system to study complex disease risks, fitness, aging, and longevity. Trends Cardiovasc Med 2013;22:29–34.
10. Valla J, Schneider L, Niedzielko T, et al. Impaired platelet mitochondrial activity in Alzheimer's disease and mild cognitive impairment. Mitochondrion 2006;6:323–330.
11. Moreira PI, Santos MS, Seica R, et al. Brain mitochondrial dysfunction as a link between Alzheimer's disease and diabetes. J Neurol Sci 2007;257:206–214.
12. Johnson GV, Stoothoff WH. Tau phosphorylation in neuronal cell function and dysfunction. J Cell Sci 2004;117:5721–5729.
13. Li L, Holscher C. Common pathological processes in Alzheimer disease and type 2 diabetes: a review. Brain Res Rev 2007;56:384–402.
14. Miklossy J, Qing H, Radenovic A, et al. Beta amyloid and hyperphosphorylated tau deposits in the pancreas in type 2 diabetes. Neurobiol Aging 2010;31:1503–1515.
15. Sivitz WI, Yorek MA. Mitochondrial dysfunction in diabetes: from molecular mechanisms to functional significance and therapeutic opportunities. Antioxid Redox Signal 2010;12:537–577.
16. Gibson GE, Starkov A, Blass JP, et al. Cause and consequence: mitochondrial dysfunction initiates and propagates neuronal dysfunction, neuronal death and behavioral abnormalities in age-associated neurodegenerative diseases. Biochim Biophys Acta 2010;1802:122–134.
17. Hinder LM, Vivekanandan-Giri A, McLean LL, et al. Decreased glycolytic and tricarboxylic acid cycle intermediates coincide with peripheral nervous system oxidative stress in a murine model of type 2 diabetes. J Endocrinol 2013;216:1–11.
18. Bosetti F, Brizzi F, Barogi S, et al. Cytochrome c oxidase and mitochondrial F1F0-ATPase (ATP synthase) activities in platelets and brain from patients with Alzheimer's disease. Neurobiol Aging 2002;23:371–376.
19. Olsson AH, Yang BT, Hall E, et al. Decreased expression of genes involved in oxidative phosphorylation in human pancreatic islets from patients with type 2 diabetes. Eur J Endocrinol 2011;165:589–595.
20. Soyal SM, Felder TK, Auer S, et al. Greatly extended PPARGC1A genomic locus encodes several new brain-specific isoforms and influences Huntington disease age of onset. Hum Mol Genet 2012;21:3461–3473.
21. Johri A, Starkov AA, Chandra A, et al. Truncated peroxisome proliferator-activated receptor-gamma coactivator 1alpha splice variant is severely altered in Huntington's disease. Neurodegener Dis 2011;8:496–503.
22. Lin J, Wu PH, Tarr PT, et al. Defects in adaptive energy metabolism with CNS-linked hyperactivity in PGC-1alpha null mice. Cell 2004;119:121–135.
23. Mootha VK, Lindgren CM, Eriksson KF, et al. PGC-1alpha-responsive genes involved in oxidative phosphorylation are coordinately downregulated in human diabetes. Nat Genet 2003;34:267–273.
24. St-Pierre J, Drori S, Uldry M, et al. Suppression of reactive oxygen species and neurodegeneration by the PGC-1 transcriptional coactivators. Cell 2006;127:397–408.

25. Choi J, Batchu VV, Schubert M, et al. A novel PGC-1alpha isoform in brain localizes to mitochondria and associates with PINK1 and VDAC. Biochem Biophys Res Commun 2013;435:671–677.
26. Ekstrand MI, Falkenberg M, Rantanen A, et al. Mitochondrial transcription factor A regulates mtDNA copy number in mammals. Hum Mol Genet 2004;13:935–944.
27. Silva JP, Kohler M, Graff C, et al. Impaired insulin secretion and beta-cell loss in tissue-specific knockout mice with mitochondrial diabetes. Nat Genet 2000;26:336–340.
28. Wang R, Li JJ, Diao S, et al. Metabolic stress modulates Alzheimer's beta-secretase gene transcription via SIRT1-PPARgamma-PGC-1 in neurons. Cell Metab 2013;17:685–694.
29. Khan RS, Fonseca-Kelly Z, Callinan C, et al. SIRT1 activating compounds reduce oxidative stress and prevent cell death in neuronal cells. Front Cell Neurosci 2012;6:63.
30. Jiang M, Wang J, Fu J, et al. Neuroprotective role of Sirt1 in mammalian models of Huntington's disease through activation of multiple Sirt1 targets. Nat Med 2011;18:153–158.
31. Vidoni ED, Van Sciver A, Johnson DK, et al. A community-based approach to trials of aerobic exercise in aging and Alzheimer's disease. Contemp Clin Trials 2012;33:1105–1116.
32. Yu F, Thomas W, Nelson NW, et al. Impact of 6-month aerobic exercise on Alzheimer's symptoms. J Appl Gerontol. 201x;xx:1–17.
33. Frahm J, Haase A, Matthaei D. Rapid three-dimensional MR imaging using the FLASH technique. J Comput Assist Tomogr 1986;10:363–368.
34. Haase A, Frahm J, Matthaei D, et al. MR imaging using stimulated echoes (STEAM). Radiology 1986;160:787–790.
35. Gruetter R. Automatic, localized in vivo adjustment of all first- and second-order shim coils. Magn Reson Med 1993;29:804–811.
36. Hennig J, Nauerth A, Friedburg H. RARE imaging: a fast imaging method for clinical MR. Magn Reson Med 1986;3:823–833.
37. Price WS, Arata Y. The manipulation of water relaxation and water suppression in biological systems using the water-PRESS pulse sequence. J Magn Reson B 1996;112:190–192.
38. Paxinos G, Watson C. The mouse brain in stereotaxic coordinates. 6th ed. New York: Academic Press, 2007.
39. Wolf OT, Dyakin V, Vadasz C, et al. Volumetric measurement of the hippocampus, the anterior cingulate cortex, and the retrosplenial granular cortex of the rat using structural MRI. Brain research. Brain Res Brain Res Protoc 2002;10:41–46.
40. Bogaert YE, Sheu KF, Hof PR, et al. Neuronal subclass-selective loss of pyruvate dehydrogenase immunoreactivity following canine cardiac arrest and resuscitation. Exp Neurol 2000;161:115–126.
41. Wittig I, Karas M, Schagger H. High resolution clear native electrophoresis for in-gel functional assays and fluorescence studies of membrane protein complexes. Mol Cell Proteomics 2000;6:1215–1225.
42. Marjanska M, Curran GL, Wengenack TM, et al. Monitoring disease progression in transgenic mouse models of Alzheimer's disease with proton magnetic resonance spectroscopy. Proc Natl Acad Sci USA 2005;102:11906–11910.
43. Xu S, Zhuo J, Racz J, et al. Early microstructural and metabolic changes following controlled cortical impact injury in rat: a magnetic resonance imaging and spectroscopy study. J Neurotrauma 2011;28:2091–2102.
44. Provencher SW. Automatic quantitation of localized in vivo ^{1}H spectra with LCModel. NMR Biomed 2001;14:260–264.
45. Ke YD, Delerue F, Gladbach A, et al. Experimental diabetes mellitus exacerbates tau pathology in a transgenic mouse model of Alzheimer's disease. PLoS One 2009;4:e7917.
46. Seifert EL, Bastianelli M, Aguer C, et al. Intrinsic aerobic capacity correlates with greater inherent mitochondrial oxidative and H_2O_2 emission capacities without major shifts in myosin heavy chain isoform. J Appl Physiol 1985;2012:1624–1634.
47. Thyfault JP, Rector RS, Uptergrove GM, et al. Rats selectively bred for low aerobic capacity have reduced hepatic mitochondrial oxidative capacity and susceptibility to hepatic steatosis and injury. J Physiol 2009;587:1805–1816.
48. Sapolsky RM. Cellular defenses against excitotoxic insults. J Neurochem 2001;76:1601–1611.
49. Mark LP, Prost RW, Ulmer JL, et al. Pictorial review of glutamate excitotoxicity: fundamental concepts for neuroimaging. Am J Neuroradiol 2001;22:1813–1824.
50. Yoshiyama Y, Higuchi M, Zhang B, et al. Synapse loss and microglial activation precede tangles in a P301S tauopathy mouse model. Neuron 2007;53:337–351.
51. Paula-Lima AC, De Felice FG, Brito-Moreira J, et al. Activation of GABA receptors by taurine and muscimol blocks the neurotoxicity of beta-amyloid in rat hippocampal and cortical neurons. Neuropharmacology 2005;49:1140–1148.
52. Wu H, Jin Y, Wei J, et al. Mode of action of taurine as a neuroprotector. Brain Res 2005;1038:123–131.
53. Santa-Maria I, Hernandez F, Moreno FJ, et al. Taurine, an inducer for tau polymerization and a weak inhibitor for amyloid-beta-peptide aggregation. Neurosci Lett 2007;429:91–94.
54. Thurston JH, Sherman WR, Hauhart RE, et al. Myo-inositol: a newly identified nonnitrogenous

osmoregulatory molecule in mammalian brain. Pediatr Res 1989;26:482–485.
55. Ripps H, Shen W. Review: taurine: a "very essential" amino acid. Mol Vis 2012;18:2673–2686.
56. Du AT, Schuff N, Amend D, et al. Magnetic resonance imaging of the entorhinal cortex and hippocampus in mild cognitive impairment and Alzheimer's disease. J Neurol Neurosurg Psychiatry 2001;71:441–447.
57. Walter A, Korth U, Hilgert M, et al. Glycerophosphocholine is elevated in cerebrospinal fluid of Alzheimer patients. Neurobiol Aging 2004;25:1299–1303.
58. Farber SA, Slack BE, Blusztajn JK. Acceleration of phosphatidylcholine synthesis and breakdown by inhibitors of mitochondrial function in neuronal cells: a model of the membrane defect of Alzheimer's disease. FASEB J 2000;14:2198–2206.
59. Kerchner GA, Hess CP, Hammond-Rosenbluth KE, et al. Hippocampal CA1 apical neuropil atrophy in mild Alzheimer disease visualized with 7-T MRI. Neurology 2010;75:1381–1387.
60. Hoxworth JM, Xu K, Zhou Y, et al. Cerebral metabolic profile, selective neuron loss, and survival of acute and chronic hyperglycemic rats following cardiac arrest and resuscitation. Brain Res 1999;821:467–479.
61. Churchwell JC, Morris AM, Musso ND, et al. Prefrontal and hippocampal contributions to encoding and retrieval of spatial memory. Neurobiol Learn Mem 2010;93:415–421.
62. Wikgren J, Mertikas GG, Raussi P, et al. Selective breeding for endurance running capacity affects cognitive but not motor learning in rats. Physiol Behav 2012;106:95–100.
63. Tweedie C, Romestaing C, Burelle Y, et al. Lower oxidative DNA damage despite greater ROS production in muscles from rats selectively bred for high running capacity. Am J Physiol Regul Integr Comp Physiol 2011;300:R544–R553.
64. Aquilano K, Baldell S, Pagliei B, et al. Extranuclear localization of SIRT1 and PGC-1alpha: an insight into possible roles in diseases associated with mitochondrial dysfunction. Curr Mol Med 2013;13:140–154.
65. Aquilano K, Vigilanza P, Baldelli S, et al. Peroxisome proliferator-activated receptor gamma co-activator 1 alpha (PGC-1alpha) and sirtuin 1 (SIRT1) reside in mitochondria: possible direct function in mitochondrial biogenesis. J Biol Chem 2010;285:21590–21599.
66. Chen J, Zhou Y, Mueller-Steiner S, et al. SIRT1 protects against microglia-dependent amyloid-beta toxicity through inhibiting NF-kappaB signaling. J Biol Chem 2005;280:40364–40374.
67. Ramadori G, Lee CE, Bookout AL, et al. Brain SIRT1: anatomical distribution and regulation by energy availability. J Neurosci 2005;28:9989–9996.
68. Biason-Lauber A, Boni-Schnetzler M, Hubbard BP, et al. Identification of a SIRT1 mutation in a family with type 1 diabetes. Cell Metab 2013;17:448–455.
69. Kilbride SM, Gluchowska SA, Telford JE, et al. High-level inhibition of mitochondrial complexes III and IV is required to increase glutamate release from the nerve terminal. Mol Neurodegener 2011;6:53.
70. Mosconi L. Brain glucose metabolism in the early and specific diagnosis of Alzheimer's disease. FDG-PET studies in MCI and AD. Eur J Nucl Med Mol Imaging 2005;32:486–510.
71. Ramsden M, Kotilinek L, Forster C, et al. Age-dependent neurofibrillary tangle formation, neuron loss, and memory impairment in a mouse model of human tauopathy (P301L). J Neurosci 2005;25:10637–10647.
72. Melov S, Adlard PA, Morten K, et al. Mitochondrial oxidative stress causes hyperphosphorylation of tau. PLoS One 2007;20:e536.
73. Santacruz K, Lewis J, Spires T, et al. Tau suppression in a neurodegenerative mouse model improves memory function. Science 2005;309:476–481.

Supporting Information

Additional Supporting Information may be found in the online version of this article:

Figure S1. Immunoelectron microscopy showing colocalization of mitochondrial p-Tau Ser396 (A) or Ser404 (B) with the voltage-dependent anion channel (VDAC), a mitochondrial marker. White and black arrows indicate VDAC (5 nm) and p-Tau Ser396 (10 nm) or p-Tau Ser404 (10 nm) immunogold labeling in LCR rat hippocampal tissue.

Figure S2. Western blot analysis of extracts from LCR rat hippocampal mitochondria using Tau (phosphor-Ser396 or 404) antibody (lanes 1 and 2) and the same antibody preincubated with blocking peptide (lane 3). Antibody was preincubated with phosphopeptide that was derived from human Tau around the phosphorylation site of serine 396 (A) or 404 (B). The synthesized phosphopeptide was derived from human Tau around the phosphorylation site of serine 396 (Y-K-S(p)-P-V) or 404 (D-T-S(p)-P-R). Lanes 1 and 3, untreated extracts of LCR rat hippocampal mitochondria: lane 2, lambda protein phosphatase treated extracts of LCR rat hippocampal mitochondria.

